JOURNAL OF MATERIALS SCIENCE: MATERIALS IN MEDICINE 4 (1993) 86–94

Synthetic silicate sulphate apatite: mechanical properties and biocompatibility testing

K. S. LESHKIVICH, E. A. MONROE
Alfred University, Alfred, NY 14802, USA

The solid solution series of $Ca_{10}(PO_4)_6F_2$–$Ca_{10}(SiO_4)_3(SO_4)_3F_2$ was synthesized by solid-state methods. Tensile strength testing by diametral compression indicated that the silicate sulphate apatites have strength comparable with that of phosphate apatite, with the centre member of the solid solution series [$Ca_{10}(PO_4)_3(SiO_4)_{1.5}(SO_4)_{1.5}F_2$] having the highest tensile strength of 20.7 MN m^{-2}. The *in vivo* behaviour of three compositions was evaluated. These materials have increased resorption rate compared with phosphate apatite, and good biocompatibility. The silicatian sulphatian apatites appear to be excellent materials for low-load-bearing bone graft applications.

1. Introduction

Compositions in the apatite solid solution $Ca_{10}(PO_4)_6F_2$–$Ca_{10}(SiO_4)_3(SO_4)_3F_2$ have not previously been synthesized as a ceramic or investigated concerning their application as a biomaterial, with the exception of the phosphate apatite end-member. Although the existence of natural silicophosphates, silicosulpho-phosphates and silicosulphate apatites is known [1–6], only limited synthesis studies have been reported [7–9].

From a bioceramic viewpoint this solid solution series involving the isomorphic substitution of the PO_4 group by SiO_4 and SO_4 is of interest because of the role that Si may play in an apatite when used as a bone graft material. Evidence has been accumulated by Carlisle [10] to show that Si performs an important role in the normal metabolism of bone and cartilage. It affects the rate of bone mineralization and appears to play a metabolic role in connective tissue and in the sequence of events leading to calcification of bone. The presence of silicon in an implant material could catalyse the mineralization process at the active site of resorption of the implant.

Fluorine is present in amounts of 30–3000 p.p.m. [5] in human tooth enamel and has long been known to increase resistance to caries attack. Fluorine tends to increase the crystallite size, due to the increased crystal growth rate, resulting in a decreased strain on the apatite lattice and increased stability of the apatite structure [11]. In addition, the solubility of fluoride apatite is reduced [12].

Both silica and sulphur are found as trace elements in human hard tissue [13]. Silica is found in amounts of 100–450 p.p.m. and sulphur in the range 100–560 p.p.m. Sulphur is found in the organic component of bone. Collagen fibres, 90% of the organic matrix of bone, are surrounded by a ground substance containing polysaccharides such as chondroitin sulphate, sialic acid and hyaluronic acid combined with various types of proteins. These proteins are made up of amino acids such as cystine, which contains sulphur.

Apatite has been investigated as a biomaterial for many years, since it is the natural bone and tooth mineral [14–17]. The biocompatibility of glass and glass ceramics has been investigated. Hench *et al.* [18] and Gross and Strunz [19] studied the anchoring of glass and glass ceramics. They found the development of an interfacial layer that is included in the remodelling of the bone and aids in advanced wound healing in the bone.

The objective of this research was to synthesize and study the mechanical and *in vivo* behaviour of this solid solution series. Material properties such as the solubility in water, free energy of formation and melting point have been investigated and are reported elsewhere.

2. Experimental

2.1. Solid-state synthesis

The solid solution series from $Ca_{10}(PO_4)_6F_2$ to $Ca_{10}(SiO_4)_3(SO_4)_3F_2$ was synthesized by solid-state methods. Six compositions were studied: $Ca_{10}(PO_4)_{6-x}(SiO_4)_{x/2}(SO_4)_{x/2}F_2$ with $x = 0$, 1.5, 3, 4, 4.5 and 6.

The solid-state synthesis was based on the reaction

$$u\text{CaO} + \text{CaF}_2 + x\text{SiO}_2 + y\text{CaSO}_4 + z\text{Ca}_3(\text{PO}_4)_2 \rightarrow \text{Ca}_{10}(\text{Si,S,PO}_4)_6\text{F}_2$$

where $x + y + 2z = 6$ in the correct stoichiometry for the selected composition, and $u + y + 3z + 1 = 10$. The reactants were $(NH_4)_2SO_4$ and $Ca(OH)_2$ (Alfa Morton Thiokal), $CaHPO_4$ (Baker Chemical Co.), CaF_2 (Fisher Scientific) and dehydrated silica gel.

The dehydrated silica gel was made by forming a gel by addition of HNO_3 to Ludox AS-40 (Dupont DeNemours and Co.) to adjust the pH to 5.27. The

0957–4530

solution was heated to 60 °C and stirred on a hotplate. Gelling occurred within 20 min, and the gel was subsequently dried in an oven at 150 °C for 24 h. The resultant dried gel was fired at 800 °C for 12 h and then ground to < 100 mesh.

The reactants, except for CaF_2, were mixed together in the theoretical stoichiometric proportions using a mortar and pestle. The mixture was prereacted at 700 °C for 2 h, forming the intermediate compounds CaO, $CaSO_4$, SiO_2 and $Ca_3(PO_4)_2$. The products were then reground using a mortar and pestle. Two subsequent firings and regrindings were performed at 800 and 900 °C for 15 h each. CaF_2 was then added to the intermediate material and the reactants were reground and pressed into pellets. The pellets were fired in a closed alumina crucible at 1000 °C for 2 h.

Powder material was ground and sieved to < 230 mesh. Using a mortar and pestle, 2 g of this powder was mixed with 10 wt% poly(vinyl alcohol). The powders were then pressed in a die of 0.75 in. (19 mm) radius to 10 000 lb (4.5 t) with a Carver press. The discs were fired slowly to 500 °C at a rate of 2.5 °C min^{-1}. The pressed discs were placed on alumina plates surrounded by CaF_2 powder, with an alumina crucible inverted over them. The discs were thus sintered in a CaF_2 atmosphere at a temperature that was 85% of the melting point determined by differential thermal analysis (DTA). After sintering, the discs were ground so that the faces were parallel, and were polished to 1 μm, then ultrasonically cleaned in methanol and dried.

The fired discs of 0% P ($x = 3$), 50% P ($x = 1.5$) and 100% P ($x = 0$) were cut with a diamond saw to sizes of 1 mm × 3 mm × 4 mm. Controls of solid Teflon were also cut to the same size as the ceramic samples. A Teflon and a ceramic sample piece were then heated on a hotplate to 240 °C to sinter the Teflon on to the surface of the ceramic sample. The implant samples were sterilized overnight in an oven at 260 °C.

2.2. Stoichiometry

The stoichiometry of the products was determined by gravimetric chemical analysis and an F-ion selective electrode. Ca was determined by the ammonium oxalate–oxalic acid method of Hillebrand [20], with Ca determined as calcium oxalate monohydrate precipitated at pH 5.0. Phosphorus was determined as magnesium phosphate ignited to pyrophosphate ($Mg_2P_2O_7$) by the method of Hillebrand. Sulphur was determined using Leco apparatus (Leco Corporation). Silicon was determined by the method of boric acid–perchloric acid mixture and weighed as precipitated silica [9].

2.3. Determination of the melting point by DTA

To determine the correct sintering temperature for the individual compositions, DTA traces were collected for powder samples on a DuPont 9900 thermal analyser at a heating rate of 10 °C min^{-1} in air. The melting point of each composition was determined by the inflection point in the high-temperature endothermic peak.

2.4. X-ray diffraction (phase identification)

Powder X-ray diffraction (XRD) data were collected on a Philips X-ray diffractometer (Philips Norelco) from 10 to 60° of 2θ at a scanning interval of 0.02° of 2θ with counting time of 1 s. The phase purity was determined for a material by comparing its diffraction pattern with Joint Committee on Powder Diffraction Standards patterns for fluorapatite.

2.5. Density and microstructure

The bulk density of the specimens was determined by American Society for Testing and Materials method C373-72: Water absorption, bulk density, apparent porosity, and apparent specific gravity of fired whiteware products.

Selected samples of each composition were examined using scanning electron microscopy (SEM) after mechanical breakage. The average particle size was determined by the line-intercept method from SEM micrographs. Approximately 200 grains were counted for each composition.

2.6. Mechanical properties

The samples were mechanically tested at room temperature, using the diametral compression test, on an Instron testing machine with a 2500 kg load cell and a crosshead speed of 5 mm min^{-1}. One face of each disc was covered with Scotch brand cellophane tape to retain the sample configuration after testing. To reduce the high compressive stresses at the loading lines, the load was distributed by inserting a pad of soft material (index card) between the loading plate and the specimens. The maximum tensile stress that occurred on the diametral planes between the loading points is given by

$$S = 2P/Dt\pi$$

where P is the applied load, D is the sample diameter and t is the sample thickness.

2.7. Biocompatibility testing

The fired discs were cut with a diamond saw to sizes of 1 mm × 3 mm × 4 mm. Controls were also cut to the same size as the samples, from solid Teflon, which is a standard inert biocompatible material. A Teflon and a ceramic sample piece were then heated on a hotplate to 240 °C to sinter the Teflon on to the surface of the ceramic sample. The implant samples were sterilized overnight in an oven at 260 °C.

2.7.1. Surgical procedure

Samples of selected compositions 0%, 50% and 100% P were implanted in the midshaft of the femur as well as subcutaneously in 10 white rats. Four samples were placed in each rat. The rats were anaesthetized with

Ketamine (Bristol Laboratory) and Rompun (Mobay Corporation). The skin over the femur and four dorsal subcutaneous sites was shaved and scrubbed with 10% providone–iodine antiseptic and cleaned with ethanol. The dorsal subcutaneous samples were placed in pockets prepared longitudinally in the back. The muscle over the femur was blunt dissected to the bone.

A cavity approximately 2 mm × 4.5 mm was drilled through the lateral cortex, medulla and medial cortex of the exposed portion of the femur with a no. 6 round dental burr. During the drilling procedure the area was continuously flushed with physiological saline solution. The implant samples protruded slightly from the cavity or were flush with the periosteum (Fig. 1). The wound was closed with independent surgical sutures. The limbs were not immobilized, and the rats were killed at 4 and 8 weeks post-operative.

2.8. Histological study

2.8.1. Soft tissue

The soft-tissue implants were removed along with the surrounding tissues of an approximate size of 4 mm × 4 mm × 4 mm. The samples were placed in 70% ethyl alcohol for 10 min and then processed through a dehydration schedule of alcohols. The dehydrated samples were then embedded into paraffin blocks and microtomed into ribbons. The tissue sections were then carefully positioned on slides, dried overnight in an oven at 37 °C and stained with haemotoxylin (Fisher Scientific) and eosin (Paragon) dyes to aid in the definition of cellular structures. After staining and air-drying, the slides were covered with Histoclad (Fisher Scientific).

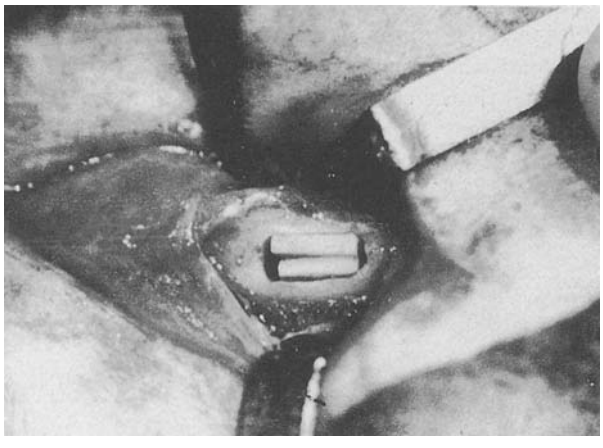

Figure 1 Ceramic sample and Teflon control "sandwich" placed in the cavity in the femur.

2.8.2. Hard tissue

The soft tissues were dissected away carefully and as completely as possible from the femur to provide for the best penetration of the fixative. The periosteum and any periosteal tissue reaction was preserved. The femur segment was initially dehydrated in 70% ethyl alcohol for 10 min. The samples were then further dehydrated through a series of dehydrations in ethyl alcohol and acetone. After final dehydration in 100% acetone, the specimens were infiltrated in Spurr (Spurr Polysciences) embedding medium. After the final embedding compound was utilized, the samples were placed in an oven at 70 °C and allowed to polymerize completely into a hard plastic.

A precision diamond Buehler Isomet low-speed saw (Buehler Ltd) was used to cut 1 mm thin sections from the plastic specimen blocks. Each specimen block was oriented before cutting to produce a section through both the ceramic and the Teflon control with the adjacent bone. After diamond-cutting the sections, one cut surface was polished and the section was mounted on a petrographic slide with balsam. The mounted sections were then ground and polished through a series of grits with a final 6 μm alumina polishing powder to a thickness of approximately 10 μm. Before examination with an optical microscope, the thin sections were stained with haemotoxylin and eosin dyes.

Selected specimens of hard-tissue implants were selected for examination with SEM (ETEC Corporation) and energy-dispersive spectroscopic (EDS) evaluation of the implant and the surrounding bone (take-off angle 35°, probe current 1×10^{-9} A, condensor lens current 2.1 A and accelerating voltage 20 kV). The Ca, P, Si and S contents of the implant, new bone and old cortical bone were examined.

3. Results

3.1. Stoichiometry

The stoichiometries of the compositions investigated are indicated in Table I. The stoichiometry was within 0.1 mol of the theoretical composition.

Stoichiometry (mol per unit cell)

	Composition [mol% P versus (Si,S)]					
Ion	$P_0(Si,S)_{100}$	$P_{25}(Si,S)_{75}$	$P_{33}(Si,S)_{67}$	$P_{50}(Si,S)_{50}$	$P_{75}(Si,S)_{25}$	$P_{100}(Si,S)_0$
Si	3.195	2.44	1.97	1.52	0.78	0.0
S	2.997	2.32	2.18	1.67	0.85	0.0
P	0.0	1.20	2.05	2.97	4.46	6.02
Ca	9.828	9.82	9.81	9.88	9.79	10.14
Ca:(P,Si,S)	1.59	1.65	1.58	1.60	1.60	1.68

3.2. Determination of melting point by DTA

The DTA patterns for the selected compositions are illustrated in Fig. 2. The melting points determined from the inflection point in the endothermic portion of the curves above 900 °C are listed in Table II.

The general trend is a lowering of the melting point with increasing substitution of Si and S for P through the solid solution series. This trend may be explained by weakening of the electrostatic bonds within the structure with increased (Si,S) substitution for P resulting in expansion of the lattice, as shown by the lattice constants, resulting in a lowered melting point for the solid.

3.3. X-ray diffraction (phase identification)

XRD data showed phase purity in the majority of samples. For a few samples of compositions with (Si,S) > P development of a second phase was noted.

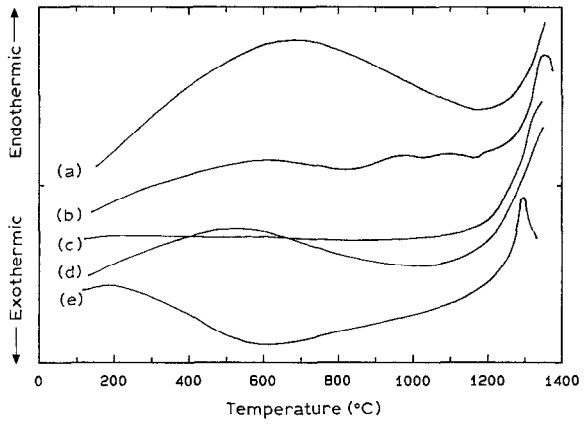

Figure 2 DTA for solid solution series: (a) 75% P, (b) 50% P, (c) 33% P, (d) 25% P and (e) 0% P.

TABLE II Melting points of solid solution compositions

Composition	Composition	Melting point (°C)
P_{100}	$Ca_{10}(PO_4)_6F_2$	1500
$P_{75}(Si,S)_{25}$	$Ca_{10}(PO_4)_{4.5}(SiO_4)_{0.75}(SO_4)_{0.75}F_2$	1250
$P_{50}(Si,S)_{50}$	$Ca_{10}(PO_4)_{3.0}(SiO_4)_{1.5}(SO_4)_{1.5}F_2$	1245
$P_{33}(Si,S)_{67}$	$Ca_{10}(PO_4)_2(SiO_4)_2(SO_4)_2F_2$	1180
$P_{25}(Si,S)_{75}$	$Ca_{10}(PO_4)_{1.5}(SiO_4)_{2.25}(SO_4)_{2.25}F_2$	1160
$P_0(Si,O)_{100}$	$Ca_{10}(SiO_4)_3(SO_4)_3F_2$	1130

This phase was identified as $Ca_4F_2Si_2O_7$ and the proposed reaction is

$$3Ca_{10}(SiO_4)_3(SO_4)_3F_2 + CaF_2 \rightarrow 3Ca_4F_2Si_2O_7 + Ca_{10}(SiO_4)_3(SO_4)_3F_2 + 3CaO + 6CaSO_4$$

Samples in which this second phase was detected were not used for mechanical or biocompatibility testing. The XRD patterns of the compositions tested are shown in Fig. 3.

3.4. Density and microstructure

The densities of the samples fired in an atmosphere of CaF_2 are listed in Table III. For comparison the densities of samples fired in an air atmosphere versus a CaF_2 atmosphere are also listed. The samples fired in an air atmosphere did not have consistent densities with similar firing conditions for repeated trials, and generally were not well sintered. Samples that were not sintered well, with low densities, had a corresponding low F content (1.86 mol) compared with the samples that were well sintered (1.99 mol F). Additionally, the average grain size of samples fired in air was 2.97 μm compared with 7.26 μm for samples fired in CaF_2 atmosphere. The CaF_2 served to aid in sintering of the samples by maintaining the correct F stoichiometry of the samples by preventing CaF_2 sublimation from the sample.

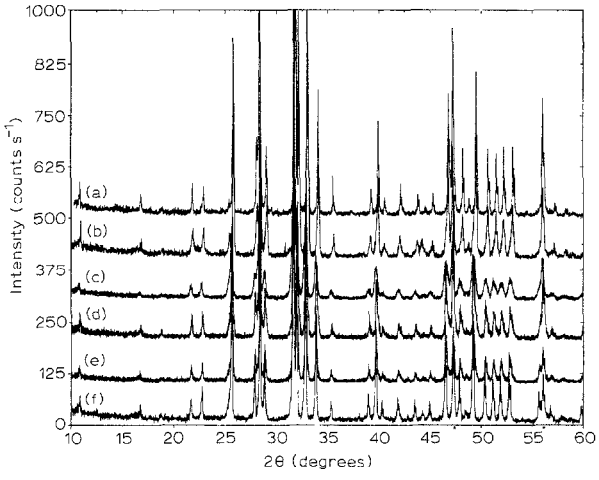

Figure 3 XRD pattern of solid solution series. $(Si,S)_{100-x}P_x$; x = (a) 100, (b) 75, (c) 50, (d) 33, (e) 25 and (f) 0.

TABLE III Densities of sintered bioceramic samples

Composition (% P)	Density (g cm^{-3})	Theoretical density (g cm^{-3})	Fired in CaF_2 atmosphere (% theoretical density)	Fired in air atmosphere (% theoretical density)
0 $Ca_{10}(SiO_4)_3(SO_4)_3F_2$	2.92 ± 0.05	3.12	94 ± 2.12	65 ± 3.0
25	2.94 ± 0.02	3.13	94 ± 0.69	81 ± 2.5
33	2.96 ± 0.07	3.14	94 ± 2.31	69 ± 2.0
50	2.94 ± 0.08	3.16	93 ± 3.00	70 ± 2.5
75	3.06 ± 0.02	3.18	96 ± 0.80	71 ± 2.3
100 $Ca_{10}(PO_4)_6F_2$	2.89 ± 0.08	3.18	94 ± 2.81	89 ± 3.0

The bioceramic samples were well sintered. The average particle sizes of the compositions are listed in Table IV. In general, the grains were of lath-type configuration. The average size of the grains increased with increasing P content of the compositions.

3.5. Mechanical properties

The tensile strengths obtained by diametral compression testing for the compositions are listed in Table V. The diametral compression test, also known as the splitting tension test or the Brazilian test [21], minimizes the influence of surface flaws and does not require elaborate fixtures. The maximum tensile stress is developed normal to the loading direction across the loading diameter. Both surface and volume flaws contribute to failure. The stress on teeth and bones is similar to those of the diametral test.

A successful padding material as bearing pads leads to tensile failures in which the sample splits into two half-cylinders along the loaded diameter. Often the tested samples broke in the triple-cleft mode, in which the sample splits symmetrically about the loaded diameter into four pieces instead of the usual or predicted half-cylinders. Both simple tensile and triple-cleft mode demonstrate tensile failures from which tensile strengths can be calculated. Shear failures and shattering of the samples were indicative of excessively high stress at the loading lines, and the results for samples exhibiting this were not used.

To normalize the data to compensate for the various densities of the compositions, the data are presented as (tensile strength/density). Fig. 4 indicates a slight trend of increased strength towards the centre member of the solid solution series. Statistical evaluation of the results (Table VI), using Student's t-test, indicated that differences in means between the 100 and 50% P compositions are significant, whereas differences between the 0 and 50% P compositions are probably significant. Differences between the 100 and 75% P compositions as well as between the 100 and 0% P compositions are not significant.

TABLE IV Average grain size

Composition (% P)	Average grain size (μm)	σ	Length of grains (μm)	σ	Intergranular pores (μm)	σ
100	6.5	1.2	56	9.2	6.3	5.2
75	5.3	2.0	15	2.2	4.9	1.5
50	4.7	1.3	25	4.0	6.6	3.0
25	3.9	0.8	22	3.7	7.9	2.2
0	4.06	1.0	25	3.2	8.0	3.2

TABLE V Strength data (MN m^{-2})

Composition (% P)	Mean	σ	Maximum value	Minimum value	N_i
100	17.17	4.03	24.3	11.1	9
75	15.92	2.72	20.0	13.1	7
50	20.69	3.37	26.6	16.7	11
33	17.66	3.67	20.3	14.3	11
25	14.96	1.74	20.7	12.7	10
0	17.99	2.47	22.8	14.3	7

TABLE VI Statistical evaluation (Students t-test) results for tensile strength

	σ	t	0.05 Confidence level	0.10 Confidence level	Degrees of freedom	Results
100% P–75% P	4.02	0.566	1.77	1.35	13	Not significant
100% P–0% P	3.96	0.574	1.77	1.35	13	Not significant
0% P–50% P	3.50	1.58	1.77	1.35	13	Probably significant
100% P–50% P	4.27	2.087	1.75	1.34	16	Significant

$$\sigma = \left(\frac{N_1 s_1^2 + N_2 s_2^2}{N_1 + N_2 - 2}\right)^{1/2} \quad \text{and} \quad t = \frac{x_1 - x_2}{\sigma(1/N_1 + 1/N_2)^{1/2}}$$

where N_i = number in sample i, σ_i = standard deviation of sample i, x_i = mean of sample i and $(N_1 + N_2 - 2)$ number of degrees of freedom.

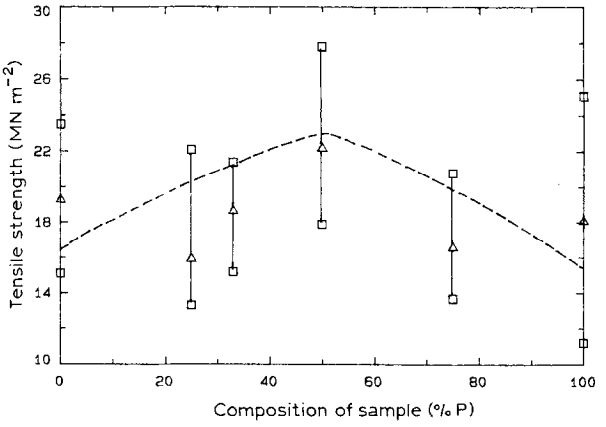

Figure 4 Tensile strength of solid solution series: (△) mean and (□) maximum and minimum values.

The strength of the compositions may be accounted for by the grain size and pore size of the samples. The compositions with (Si,S) > P generally had a smaller grain size than compositions with P > (Si,S), which would result in a higher tensile strength. However, the average pore size for these compositions of (Si,S) > P was generally greater than for samples with P > (Si,S), which would contribute to a lower tensile strength. The combined effect of these two parameters may account for the significant increase in strength of the 50% P composition.

These values are lower than tensile strength values obtained from diametral compression tests of 100% phosphate apatite by previous investigators [9] which are of the order of 37 MN m^{-2}. This overall reduction in strength values obtained in this study compared with the previous literature reports for 100% phosphate apatite is probably due to the processing technique used in fabrication of the test specimens and the microstructure. There is a consistent trend of increased strength from the end-members of the series towards the 50% P member, which reflects the compositional and microstructural changes.

3.6. Soft tissue histology

The sections were evaluated for signs of inflammatory reaction and graded as to the thickness of the fibrous tissue layer that surrounded all of the implanted samples. Measurements of the thickness of the fibrous tissue layer were obtained using a reticle under magnifications of × 2.5 and × 10. A chronic inflammation is characterized by the presence of mononuclear cells called macrophages, which may coalesce to form multinucleated giant cells. The macrophages are phagocytic and remove foreign material or bacteria. The mononuclear cells may evolve into histiocytes, which regenerate collagen. This regenerated collagen is used to wall off unremovable foreign material by encapsulation. A greater thickness of the fibrous tissue capsule is indicative of a greater irritation of the foreign material. If the fibrous capsule is thin, this indicates good biocompatibility or bio-inertness.

The microscopic examinations of the subcutaneous implant samples after 4 and 6 weeks implant duration are summarized in Table VII.

0% *P fluorellestadite.* After 4 weeks implantation the 0% P samples had a fibrous layer of average thickness 0.04 mm surrounding the ceramic sample and 0.05–1.0 mm surrounding the Teflon control sample. In one section the fibrous tissue layer had grown between the ceramic and Teflon implants. After 6 weeks implantation the fibrous layer thicknesses were comparable with those of the 4-week samples. No macrophages or giant cells were noted in any of the samples, indicating no inflammation.

50% *P.* After 4 weeks implantation the fibrous tissue capsule surrounding the ceramic was 0.02 mm compared with 0.1 mm for the Teflon control. After 6 weeks implantation the fibrous capsule was 0.05 mm surrounding the ceramic and 0.07 mm surrounding the Teflon control. There was growth of a blood vessel adjacent to the ceramic after 6 weeks implantation, indicating very good biocompatibility. Another 6-week section showed growth of the fibrous tissue into pores of the ceramic and between the ceramic and Teflon control materials. No macrophages or giant cells were evident in any of the sections.

100% *P fluorapatite.* The 100% P samples had a fibrous tissue capsule of 0.05 mm surrounding the ceramic and 0.1 mm surrounding the Teflon control after 4 weeks implantation. After 6 weeks implantation the fibrous tissue capsule was comparable with the 4-week sections. There was no evidence of

TABLE VII *In vivo* implants

% P	Time (weeks)	Thickness of capsule (mm), subcutaneous implant		Bone–implant direct contact (%)	
0	4	Sample	0.04 ± 0.008	Sample	50 ± 0.0
		Teflon	0.07 ± 0.19	Teflon	25 ± 15
0	6	Sample	0.04 ± 0.01	Sample	82 ± 2.5
		Teflon	0.05 ± 0.01	Teflon	25 ± 5
50	4	Sample	0.02 ± 0.01	Sample	90 ± 5
		Teflon	0.10 ± 0.01	Teflon	60 ± 7
50	6	Sample	0.05 ± 0.00	Sample	60 ± 0
		Teflon	0.07 ± 0.01	Teflon	40 ± 5
100	4	Sample	0.05 ± 0.00	Sample	50 ± 8
		Teflon	0.10 ± 0.02	Teflon	25 ± 25
100	6	Sample	0.05 ± 0.01	Sample	10 ± 0
		Teflon	0.10 ± 0.02	Teflon	0 ± 0

inflammation, which would be indicated by the presence of macrophages or giant cells.

Fig. 5 illustrates the fibrous tissue capsule that surrounded all of the implanted materials. The thickness of the capsule was consistently less for the ceramic sample than for the Teflon sample that served as the inert control material. There appeared to be a thinner capsule surrounding the 50% P samples than that for both the 0 and 100% P samples. Fibrous tissue had also grown between the sample and Teflon on both the 0 and 50% P implants. The presence of a blood vessel close to the implanted 50% P sample after 6 weeks implantation indicated good biocompatibility, with no evidence of inflammatory reaction or toxic reaction to the ions released.

3.7. Hard tissue histology: optical microscopy

The microscopic examinations of the hard tissue implanted samples after 4 and 6 weeks implantation are summarized in Table VII. The samples were evaluated for the percentage of bone–implant direct contact (based on the area of bone in direct contact with the implant divided by the total area of the bone–implant interface), and signs of inflammation.

0% *P fluorellestadite.* After 4 weeks implantation 50% of the ceramic implant surface exposed was in direct contact with the new bone. The Teflon control samples had from 10 to 40% new bone–sample direct contact. New bone had grown between the ceramic and Teflon implants. Connective tissue had grown between the Teflon control and the new bone in one section, indicating less biocompatibility. After 6 weeks implantation the ceramic had 80% new bone–sample direct contact, whereas the Teflon control had 20–30%. New bone had also grown into pores on the surface of the ceramic sample. One section fractured during preparation, but the fracture propagated through the new bone–ceramic interface rather than along the interface, indicating a very strong bond at the interface.

50% *P.* After 4 weeks implantation the ceramic sample exhibited 90% new bone–sample direct contact, whereas the Teflon control showed 60%. A crack incurred during sample preparation extended through the new bone–ceramic interface, rather than along the interface. Growth of a complete osteon including the Haversian canal up to the surface of the ceramic was noted, indicating very good biocompatibility. After 6 weeks implantation the ceramic showed 60% new bone–sample direct contact, whereas the Teflon showed 40%. Connective tissue was noted between the Teflon sample and the newly formed bone, but not between the ceramic and new bone.

100% *P fluorapatite.* After 4 weeks implantation the ceramic showed 50% direct contact with the new bone, whereas the Teflon showed from 0 to 50%. Connective tissue had formed between the Teflon and the new bone, but not between the ceramic and new bone. A fracture incurred during sample preparation propagated through the ceramic–bone interface. After 6 weeks implantation there was 0% direct contact between the ceramic and new bone and only 0–10% direct contact of new bone with the Teflon control. There was generally very little new bone growth throughout the sections.

The 0% P composition exhibited the greatest area of bone–implant direct contact, and the 100% P showed the least bone contact area of the three types of ceramic samples. In most cases there was an interlayer of connective tissue between the Teflon control and the new bone formation. There was no evidence of this interlayer between the ceramic samples and the new bone. Some samples exhibited fractures due to the sample preparation, sawing and grinding operations (Fig. 6). In these samples it is interesting to note that the fractures, originating in the ceramic, propagated through the bone–ceramic interface into the bone rather than along the interface. The conclusion was drawn that a chemical bond existed between the bony tissue and the ceramic, resulting in a stronger interface than the bulk of the ceramic.

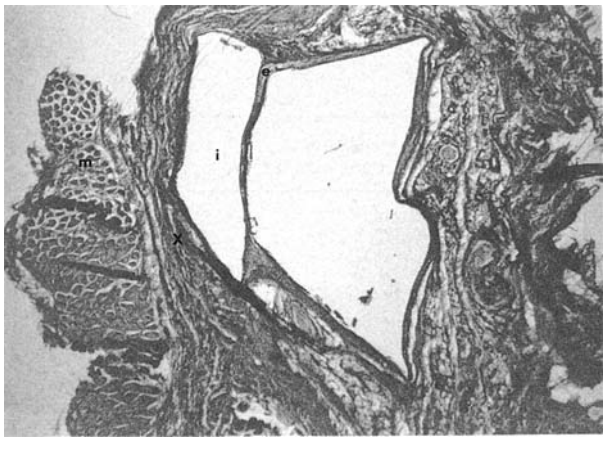

Figure 5 Soft tissue sample fibrous tissue encapsulation: i, ceramic implant; e, soft tissue encapsulation; X, surrounding soft tissue and m, muscle fibres.

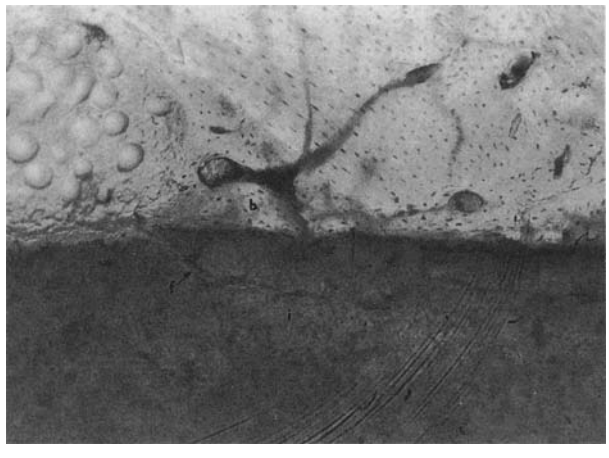

Figure 6 Hard-tissue implant, $(Si,S)_{100}P_0$, 4 weeks. Fracture through interface in hard tissue implant. Growth of complete Haversian system up to surface ceramic implant: i, ceramic implant; b, bone and f, fracture.

Particularly in the 0 and 50% P materials, it was seen that the newly formed bone matrix followed microscopic undulations in the surface of the implant samples (Fig. 7). Also indicating very good biocompatibility was the growth of complete osteons including the Haversian canals up to the surface of the implant material. Fig. 6 shows growth of the osteon up to a corner of the implanted 50% P samples after only 4 weeks implantation.

Some implant resorption was evident, particularly with the 0% P samples. Surface pores had developed, due to the high solubility of this composition into which new bony tissue had grown as shown in Fig. 7.

3.8. Hard tissue: electron microscopy and EDS

Examination of 50% P implanted samples of 6 weeks duration by EDS indicated a definite concentration gradient of both silicon and sulphur from the implanted ceramic outwards to the old bone matrix. Figs 8 and 9 show the spectra and the corresponding area examined on the implanted specimens. Spectrum number 1 corresponds to the implant, spectra 2 and 3 correspond to areas of new bone growth, and spectrum 4 corresponds to an area of old bone.

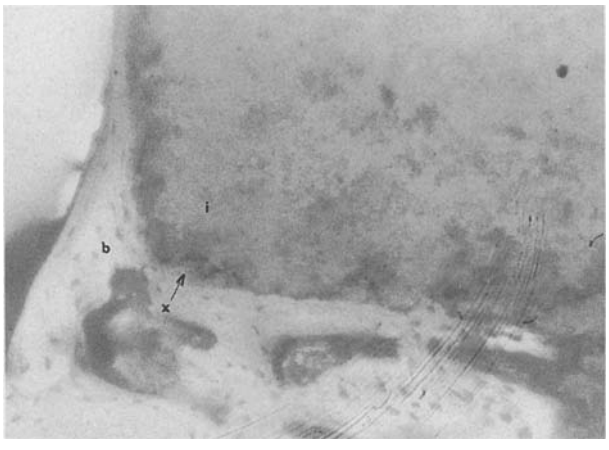

Figure 7 Hard-tissue implant, $(Si,S)_{100}P_0$, 4 weeks: i, implant; b, bone; x, bone growth into surface irregularities and pores.

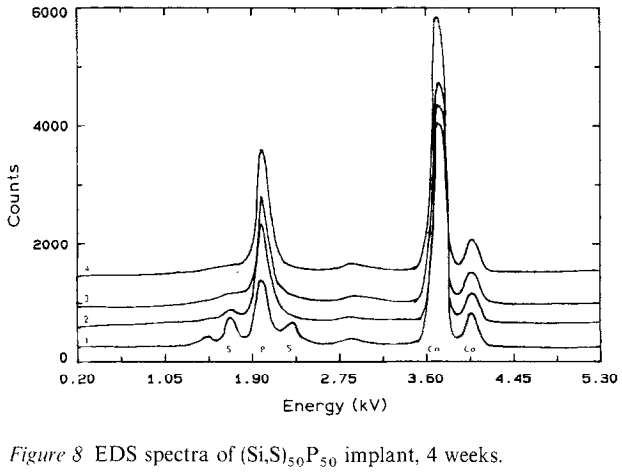

Figure 8 EDS spectra of $(Si,S)_{50}P_{50}$ implant, 4 weeks.

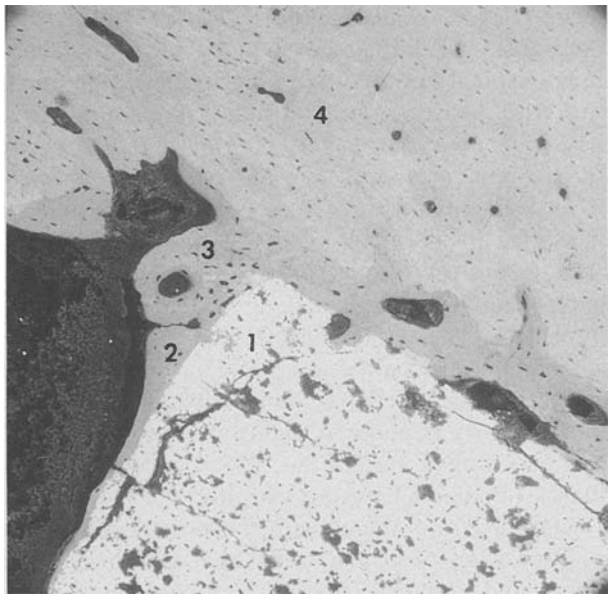

Figure 9 Area of EDS spectra $(Si,S)_{50}P_{50}$ implant, 4 weeks: 1, ceramic implant; 2, newest bone; 3, new bone and 4, mature (old) bone.

The implanted composition was 50% P, that is (Si,S):P of 1.0. New bone formed adjacent to the ceramic implant material showed a very high silicon and sulphur concentration (Si,S):P = 0.30, bone intermediate between the newly formed bone matrix adjacent to the ceramic and the old bone matrix showed an (Si,S):P = 0.15, and the old bone matrix, near the cortex of the femur, showed an (Si,S):P = 0.0. These results are consistent with recent investigations in the literature concerning the involvement of silicon in the formation of new bone tissue. The sulphur content was also high in the new bone, and although its requirements for bone formation are not known, it does not appear to prevent interfacial osteogenesis.

4. Summary

DTA indicated a decreasing melting point from 1500°C for fluorapatite to 1130°C for fluorellestadite. This decreasing melting point in conjunction with increased lattice constants *a* and *c* corresponds to decreasing bond strength from the phosphate apatite end-member to the silicate–sulphate apatite end-member. During fabrication of ceramic bodies from powders of the various compositions, firing in an atmosphere of CaF_2 improved densification by preventing the loss of POF_3 and CaF_2 from the ceramic, allowing for a reduced sintering temperature and shorter firing schedules.

Tensile strength data indicated that the silicatian sulphatian apatites have strength comparable with those of phosphate apatites, despite the suggestion that the chemical bond strengths should increase from the 0 to the 100% P end-members. The centre member of the solid solution series $[Ca_{10}(PO_4)_3(SiO_4)_{1.5}(SO_4)_{1.5}F_2]$ had the highest tensile strength of 20.69 MN m^2.

In vivo animal biocompatibility testing showed the silicatian sulphatian end-member and the centre

member of the solid solution series to have a greater percentage of both new bone growth and new bone–implant direct contact compared with fluorapatite. Although there was an interlayer of connective tissue between the Teflon control and the newly formed bone, there was no evidence of this connective tissue formation between the ceramic implants and the new bone. From evaluation of fractures induced in the thin sections by specimen preparation, which propagated through rather than along the interface, a strong implant–bone interface had formed in the silicatian sulphatian end-member and centre member implanted samples. None of the ceramic implants elicited an inflammatory response. A slightly thinner fibrous capsule had formed around the 50% P ceramic implant than around either the 0 or the 100% P samples.

EDS spectra of the implanted centre member composition after 6 weeks showed a high concentration of silicon and sulphur in the active growth region of the new bone adjacent to the ceramic implant. As the distance from the implanted ceramic increased, corresponding to increased maturity of the bone, the concentration of silicon and sulphur decreased.

The silicatian sulphatian apatites produce an alkaline environment upon hydrolysis, releasing ions at the implant surface [22]. These materials have increased solubility and subsequent increased resorption rate *in vivo*, comparable strength and excellent biocompatibility. These silicatian sulphatian apatites appear to be excellent materials for low-load-bearing bone graft applications, such as filling holes after cleaning defects from trauma or disease in bony tissue that are still essentially surrounded by bone. Also, it has a potential as replacement for bony walls such as portions of the skull, paranasal sinuses, osseous walls of the external meatus, reconstruction of ossicular chain, etc. For these applications the implant material could be resorbed and be simultaneously replaced by newly formed bony tissue.

References

1. R. BRAUNS, *Neus Jahrb. Miner. Geol. Palosontol. Beilagaband* **4** (1917) 60.
2. K. HARADA, K. NAGASHIMA and A. KOTA, *Amer. Miner.* **56** (1971) 1507.
3. D. McCONNELL, *ibid.* **22** (1937) 977.
4. R. ROUSE and P. DUNN, *ibid.* **67** (1982) 90.
5. K. SUDARSANAN and R. YOUNG, *Acta Crystallogr.* **B34** (1978) 1401.
6. Z. VASILEVA, *Geochemistry* (1958) 464–471.
7. R. KLEMENT, *Naturwissenschaften* **27** (1939) 57.
8. R. KLEMENT and P. DIHN, *Ber. Bunsenges. Phys. Chem.* **48** (1942) 334.
9. E. KREIDLER, PhD thesis, Marquette University, Milwaukee, Wisconsin (1974).
10. E. M. CARLISLE, in "Silicon Biochemistry" (Wiley, New York, 1986) p. 123.
11. R. YOUNG and D. B. WILES, *Arch. Oral Biol.* **11** (1966) 699.
12. F. DRIESSENS, *Ber. Bunsenges. Phys. Chem.* **82** (1978) 312.
13. F. LOSEE, T. CURTRESS and R. BROWN, *Envir. Health* **7** (1973) 19.
14. H. DENISSON, C. MANGANO and G. VIENINI, in "Hydroxylapatite Implants" (Piccin Niova Libraria, Padua, 1985) p. 29.
15. P. DUCHEYNE and J. LEMONS, in "Bioceramics: Material Characteristics Versus *In Vivo* Behavior" (New York Academy of Science, New York, 1988) p. 131.
16. M. JARCHO, C. BOLEN, M. THOMAS, J. BOBICK, J. KAY and H. DOREMUS, *J. Mater. Sci.* **11** (1976) 2027.
17. M. THOMAS, R. DOREMUS, M. JARCHO and R. SALSBURY, *ibid.* **15** (1980) 891.
18. L. HENCH, R. SPLINTER, W. ALLEN and T. GREENLEE, *Mater. Res. Symp.* **2** (1971) 117.
19. U. GROSS and V. STRUNZ, *J. Biomed. Mater. Res.* **14** (1980) 607.
20. W. F. HILLEBRAND, in "Applied Inorganic Analysis" (Wiley, New York, 1953) p. 671.
21. L. MORDFIN and M. KERPER, in Mechanical and Thermal Properties of Ceramics, Symposium on the Mechanics and Thermal Properties of Ceramics Proceedings, 1968 p. 243.
22. K. LESHKIVICH, PhD thesis, Alfred University, Alfred, New York (1990).

Received 20 January 1991
and accepted 12 February 1992